Chinese Journal of Chemical Engineering 67 (2024) 16–26

Contents lists available at ScienceDirect

Chinese Journal of Chemical Engineering

journal homepage: www.elsevier.com/locate/CJChE

Full Length Article

Effect of mesopore spatial distribution of HZSM-5 catalyst on zinc state and product distribution in 1-hexene aromatization

Chenhao Wei [1], Di Gao [2], Guohao Zhang [1], Liang Zhao [1,*], Jinsen Gao [1], Chunming Xu [1]

[1] The State Key Lab of Heavy Oil Processing, China University of Petroleum (Beijing), Beijing 102249, China
[2] SINOPEC Research Institute of Petroleum Processing Co., Ltd., Beijing 100083, China

ARTICLE INFO

Article history:
Received 4 August 2023
Received in revised form
17 November 2023
Accepted 20 November 2023
Available online 4 December 2023

Keywords:
1-Hexene aromatization
Alkali treatment
Xylene selectivity
Mesopores
Zinc state

ABSTRACT

1-hexene aromatization is a promising technology to convert excess olefin in fluid catalytic cracking (FCC) gasoline to high-value benzene (B), toluene (T), and xylene. Besides, the increasing market demand of xylene has put forward higher requirements for new generation of catalyst. For increasing xylene yield in 1-hexene aromatization, the effect of mesopore structure and spatial distribution on product distribution and Zn loading was studied. Catalysts with different mesopore spatial distribution were prepared by post-treatment of parent HZSM-5 zeolite, including NaOH treatment, tetra-propylammonium hydroxide (TPAOH) treatment, and recrystallization. It was found the evenly distributed mesopore mainly prolongs the catalyst lifetime by enhancing diffusion properties but reduces the aromatics selectivity, as a result of damage of micropores close to the catalyst surface. While the selectivity of high-value xylene can be highly promoted when the mesopore is mainly distributed interior the catalyst. Besides, the state of loaded Zn was also affected by mesopores spatial distribution. On the optimized catalyst, the xylene selectivity was enhanced by 12.4% compared with conventional Zn-loaded parent HZSM-5 catalyst at conversion over 99%. It was attributed to the synergy effect of mesopores spatial distribution and optimized acid properties. This work reveals the role of mesopores in different spatial positions of 1-hexene aromatization catalysts in the reaction process and the influence on metal distribution, as well as their synergistic effect two on the improvement of xylene selectivity, which can improve our understanding of catalyst pore structure and be helpful for the rational design of high-efficient catalyst.

1. Introduction

The global wave of environmental protection and carbon dioxide emission reduction has put forward higher requirements for traditional vehicle fuels [1–3]. For example, on the one hand, various economies have stricter restrictions on olefins and aromatics content in gasoline; on the other hand, the popularity of new energy vehicles has made the demand growth for gasoline weak. To meet these challenges, traditional refineries producing fluid catalytic cracking (FCC) gasoline need to find new ways to convert excess olefins. Benzene (B), toluene (T), and xylene are important chemical raw materials, which can be used to produce fabric, rubber, medicine, *etc*. [4–6]. Among them, the demand for xylene has increased greatly in recent years due to the rapid growth in demand for its downstream products [7–9]. Therefore, the aromatization of olefins has become a necessary choice for refineries to reduce olefin content and improve economic benefits.

HZSM-5 is one of the most commonly used 1-hexene aromatization catalysts, due to its special pore structure has high selectivity to aromatics [10,11]. However, highly selective ten-membered ring channels also have diffusion limitations on aromatics that are detrimental to the catalyst's lifetime [12–14]. To prolong the lifetime of HZSM-5 in aromatization, an efficient solution is to introduce intracrystalline mesopores inside the zeolite. After mesopores are introduced, the diffusion of reaction intermediates and products can be enhanced and the coke formation can be suppressed. Groen *et al.* [15] synthesized HZSM-5 zeolite with intracrystalline mesopores by post-treatment with 0.2 mol·L^{-1} NaOH solution. It was found the characteristic diffusion path length of neopentane in the mesoporous zeolite was dramatically shortened by approximately 2 orders of magnitude. Li *et al.* [16] introduced mesopores into HZSM-5 by alkali treatment and found the aromatization

* Corresponding author.
E-mail address: liangzhao@cup.edu.cn (L. Zhao).

https://doi.org/10.1016/j.cjche.2023.11.008
1004-9541/

stability, which is defined as the ratio of aromatics selectivity at 8 h time on stream (TOS) to that at 2 h TOS, was enhanced by more than 3 times. However, due to the difference in the protocols used in creating mesopores, the introduced mesopores may vary in spatial distribution and volume. Besides, the introduced mesoporous structure will inevitably affect the yield and distribution of products. Therefore, against the backdrop of increasing emphasis on the transformation of excess fuel oil to high-value-added products, it is more urgent to study the influence of the introduction of mesopores on product distribution in 1-hexene aromatization.

In addition to introducing mesopores, another commonly used modification of the HZSM-5 aromatization catalyst is introducing zinc element [17,18]. Once Zn species are loaded, a new reaction pathway of olefins forms allylic species and then forms aromatics directly can happen, which will greatly benefit the aromatics yield [19,20]. The introduced Zn species mainly exist in two different forms of ZnO and $ZnOH^+$. Gao *et al.* [21] prepared a series of Zn-loaded HZSM-5 catalysts with different $ZnOH^+$/ZnO ratios to analyze the influence of zinc state on 1-hexene aromatization and cyclohexane dehydrogenation. It was found both the hydrogen transfer ability and the dehydrogenation ability increase linearly with the amount of surface $ZnOH^+$ species while keeping identical bulk zinc content. Thus, it is of great importance to increase the ratio of $ZnOH^+$/ZnO in Zn-loaded HZSM-5 catalysts. Researchers have found some factors that may affect the Zn state, such as the impregnation method, calcination, mechanical mixing, doping with non-metallic elements, and so on. However, it is still unclear whether and how it is affected by the introduction of mesopores.

This study concentrates on the influence of mesopore's spatial distribution and amount on product distribution and the Zn state of the 1-hexene aromatization catalyst. Post-treatment of NaOH, TPAOH solutions, and recrystallization were used to synthesize catalysts with different pore structures. The spatial distribution of introduced mesopores and the way it affects the product distribution and Zn state are systematically analyzed.

2. Experimental

2.1. Preparation of the catalysts

2.1.1. Chemical agents

Nanosized HZSM-5 (Nankai University Catalyst Plant, China) with SiO_2/Al_2O_3 ratio of 27 was chosen as the parent catalyst. 1-Hexene (99%, AR), *tetra*-propylammonium hydroxide (TPAOH, 99%, AR), $Zn(NO_3)_2\cdot 6H_2O$ (99%, AR), and NaOH (95%, AR) are purchased from Shanghai Aladdin Biochemical Technology Co., Ltd., China. All the chemicals were used without further purification.

2.1.2. Inorganic alkali-treated catalysts

Parent HZSM-5 was treated with NaOH solutions with concentrations of 0.2, 0.3, 0.4 and 0.5 $mol\cdot L^{-1}$. The treatment was performed at 90 °C with stirring for 2 h. After the treatment, the samples were filtered and dried at 120 °C overnight. Then, the samples were NH_4^+-exchanged with NH_4NO_3 solution. Finally, the samples were dried at 120 °C overnight and calcined at 550 °C for 4 h. The catalysts were named as *x*Na/Z5, where *x* represents the concentration of alkali solution used in the treatment.

2.1.3. Organic alkali-treated catalysts and recrystallized catalysts

For organic alkali-treated catalysts, the parent HZSM-5 was treated with TPAOH solutions with concentrations of 0.2, 0.3, 0.4, and 0.5 $mol\cdot L^{-1}$. All the procedures are the same as it is in inorganic alkali-treated catalysts, except for the catalysts treated with organic alkali were not NH_4^+-exchanged. The catalysts were named as *x*TPA/Z5, where *x* represents the concentration of alkali solution used in the treatment.

For recrystallized catalysts, the parent HZSM-5 catalyst was firstly treated with TPAOH as above; then, the suspension was transferred into a Teflon-lined autoclave and heated to 170 °C for h to recrystallize. After the recrystallization, the catalysts were filtered, washed, and dried at 120 °C overnight and then were calcined at 550 °C for 4 h. The catalysts were named as *x*TPA-*y*/Z5, where *x* represents the concentration of alkali solution used in the treatment and *y* represents the recrystallization time in the autoclave.

2.1.4. Zn-loaded catalysts

Since we had found the best loading amount of Zn is 3% (mass) in our previous study [21]. 3% Zn was loaded on HZSM-5, 0.4Na/Z5, 0.4TPA/Z5, and 0.4TPA-24/Z5 by equal volume impregnation method with $Zn(NO_3)_2$ solution with proper concentration. After the impregnation, the catalysts were dried at 120 °C for 8 h. Then they are calcined at 550 °C for 4 h. After loading Zn, the catalysts were named as Zn-HZSM-5, Zn-0.4Na/Z5, Zn-0.4TPA/Z5, and Zn-0.4TPA-24/Z5, where Zn represents 3% Zn loading.

2.2. Characterization of the catalysts

The catalysts' crystallographic characterizations were determined from X-ray diffraction (XRD) by using a Bruker D8 Advance X-ray diffractometer in the range of 2θ ranging from 5° to 50° at a rate of $10(^o)\cdot min^{-1}$.

The surface areas and pore volumes were calculated using the Brunauer–Emmett–Teller method from nitrogen adsorption and desorption isotherms measured with a Micromeritics ASAP 2460 instrument at −196 °C. And the *t*-plot method was used to calculate the micropore-specific surface areas and micropore volumes.

The chemical compositions of the samples were determined by an inductively coupled plasma–optic emission spectrometer (ICP–OES) using an Agilent 5110 instrument.

X-ray photoelectron spectroscopy (XPS) was conducted on a Thermo Scientific K-Alpha$^+$ spectrometer equipped with a monochromatic Al K_α X-ray source (1486.6 eV) operating at 100 W. All peaks would be calibrated with C 1s peak binding energy at 284.8 eV for adventitious carbon.

The temperature-programmed desorption of ammonia (NH_3-TPD) was carried out on a DAS-7200 chemical adsorber instrument (Huasi Instrument Co., Ltd., China). The sample was pretreated at 600 °C in a flow of nitrogen for 30 min. Subsequently, the sample was cooled to 100 °C and kept in a flow of NH_3 for 30 min. Physically adsorbed NH_3 was removed by purging the N_2 flow until the baseline recorded by the thermal conductivity detector (TCD) signal was stable. Finally, the sample was heated from 100 to 700 °C at a rate of 10 $°C\cdot min^{-1}$ in a flow of N_2, and the TCD signal was recorded.

Pyridine-adsorbed infrared (Py-IR) was used to obtain the acidic properties by using a Nicolet Avatar 360 spectrometer. After being placed in the quartz IR cell with CaF_2 windows, the sample was pretreated at 400 °C under vacuum (1.0×10^{-4} Pa) for 1 h. Subsequently, the sample was cooled to 35 °C, and the spectrum was recorded as the background. Then the valve between the cell and the pump system was closed, allowing exposure to pyridine for 5 min to adsorb pyridine. The Py-IR spectra were recorded at ambient temperature after desorbing pyridine at 200 and 350 °C, respectively. The number of total acid sites and strong acid sites was determined according to the spectra scanned after degassing at 200 and 350 °C, respectively. The number of weak acid sites was obtained by subtracting the number of strong acid sites from the total number of acid sites. The amount of External Brønsted Acid

(EBA) was measured *via* a 2,6-lutidine adsorption infrared experiment. The experimental procedures are the same as for Py-IR except that 2,6-lutidine is used as an adsorbate.

2.3. Catalyst tests and analysis methods

The aromatization of 1-hexene on these prepared catalysts was tested in a stainless-steel fixed bed reactor with an internal diameter of 13 mm. A catalyst (1.0 g) with a particle size of 40–60 mesh (0.25–0.42 mm) was placed in the isothermal zone of the reactor. All of the experiments were conducted at atmospheric pressure. Prior to the aromatization reaction, the temperature was elevated to 500 °C in a N_2 flow of 150 ml·min^{-1} for 1 h and then cooled to reaction temperature (350 °C), and the reaction was started by using the 1-hexene as the reactor feed. 1-Hexene was introduced into the reactor at a weight hourly space velocity of 0.5 h^{-1}. The product was analyzed online with an Agilent 8890B gas chromatography (GC) equipped with flame ionization detector (FID), thermal conductivity detector (TCD), and an OV-101 capillary column (50 m × 0.2 mm × 0.50 μm). The temperature of the pipeline between the GC and the reactor was kept at 200 °C to prevent product liquefaction. The analysis of the product was the average result in the first 1 h.

3. Results and Discussion

3.1. Structure and textural property

Fig. 1 shows the XRD patterns of the parent, inorganic alkali treated, organic alkali treated, recrystallized after alkali treatment, and Zn-loaded HZSM-5 catalysts. The diffraction peaks at $2\theta = 8°–10°$ and 22°–25° showed all catalysts maintain typical MFI structure [22–24]. Table 1 shows bulk and surface SiO_2/Al_2O_3 and the crystallinity of all catalysts. Combining Fig. 1(a) and Table 1, it can be concluded that when the concentration of NaOH is lower than 0.5 mol·L^{-1}, the crystal structure of HZSM-5 can be well preserved. However, as the concentration of NaOH increases, the relative crystallinity of catalysts keeps decreasing. 0.5 mol·L^{-1} NaOH treatment finally leads to only 75% crystallinity. This could be attributed to the desilication by alkali treatment [25–27]. With the increase in NaOH concentration, the effects of desilication increase. Besides, from the data obtained from ICP-OES and XPS, it can be found both bulk and surface SiO_2/Al_2O_3 decrease at the same level with the increase of NaOH concentration used in the alkali treatment. This indicates the NaOH solution functions evenly both on the surface and inside of HZSM-5 during the desilication. The same as *x*Na/Z5 catalysts, from Fig. 1(b), the organic alkali treatment will not destroy the crystal structure when the concentration of TPAOH is lower than 0.5 mol·L^{-1}.

However, from Table 1, the crystallinity did decrease with the concentration of TPAOH increase. Compared with *x*Na/Z5 catalysts, the crystallinity and SiO_2/Al_2O_3 of *x*TPA/Z5 catalysts are higher when alkali solutions with the same concentration were used. This could be explained by the truth that TPAOH is less alkaline than NaOH. Besides, comparing the data obtained by XPS and ICP-OES, the surface SiO_2/Al_2O_3 is higher than bulk SiO_2/Al_2O_3 for *x*TPA/Z5 catalysts. This is because the surface of HZSM-5 is negatively charged after the hydroxyl group losses its proton and positively charged TPA^+ will hence adsorb on the surface and hinder surface

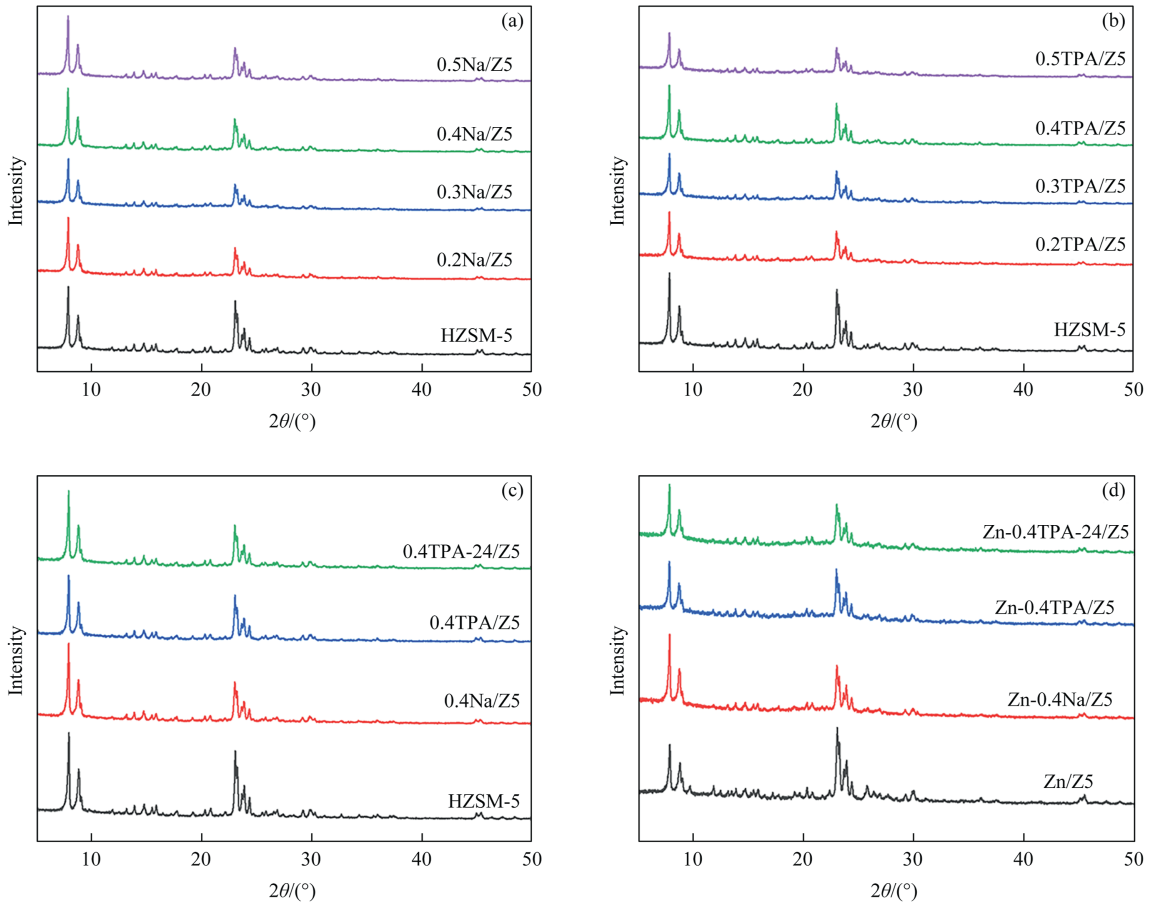

Fig. 1. XRD patterns of HZSM-5 and modified catalysts.

Table 1
SiO_2/Al_2O_3 and relative crystallinity of catalysts

Catalysts	Bulk $SiO_2/Al_2O_3$①	Surface $SiO_2/Al_2O_3$②	Relative crystallinity
HZSM-5	27	26	95%
0.2Na/Z5	25	23	92%
0.3Na/Z5	23	22	90%
0.4Na/Z5	21	20	86%
0.5Na/Z5	17	15	75%
0.2TPA/Z5	26	27	94%
0.3TPA/Z5	25	26	92%
0.4TPA/Z5	24	26	90%
0.5TPA/Z5	22	24	87%
0.4TPA-24/Z5	24	28	91%
Zn/Z5	27	26	94%
Zn-0.4Na/Z5	21	20	86%
Zn-0.4TPA/Z5	24	26	89%
Zn-0.4TPA-24/Z5	24	28	90%

① Measured by ICP-OES.
② Measured by XPS.

corrosion. Furthermore, TPA^+ cannot diffuse into the micropores of this zeolite easily due to its relatively large dimension. Therefore, the interior silicon of *x*TPA/Z5 is preferentially removed. Combining Fig. 1(c) and Table 1, one can find NaOH treatment, TPAOH treatment, and TPAOH treatment plus recrystallization all lead to the decrease of relative crystallinity and bulk SiO_2/Al_2O_3, which proves these 3 protocols all lead to desilication. Of note is that though the bulk SiO_2/Al_2O_3 of 0.4TPA/Z5 and 0.4TPA-24/Z5 are the same, the surface SiO_2/Al_2O_3 of 0.4TPA-24/Z5(28) is higher than that of 0.4TPA/Z5(26). This can be explained by that TPAOH not only functions as an alkali but it is also a commonly used template during the synthesis of HZSM-5. Therefore, the silicon removed during desilication will be crystallized on the surface of the catalyst with the help of TPA^+ during recrystallization [28,29]. And finally, the surface SiO_2/Al_2O_3 of the catalyst is enhanced. From Fig. 1(d), it can be concluded that the crystal structure will not be destroyed by loading Zn, though Table 1 shows there is a relative crystallinity drop within 1%. And no peak of ZnO appears, which indicates the good dispersion of Zn on the catalyst [30,31].

The textural properties of catalysts were determined by the N_2 adsorption and desorption isotherms. The detailed surface areas and pore volumes are listed in Table 2. For *x*Na/Z5 series, the micropore surface area and volume begin to decrease when the concentration of NaOH reached to 0.3 $mol \cdot L^{-1}$. And when it comes to 0.5 $mol \cdot L^{-1}$, the micropore surface area and volume drop sharply, implying part of the micropore structure has been destroyed by desilication [32–34]. However, the mesopore volumes increase with the increase of NaOH concentration. When the concentration of NaOH altered from 0.4 to 0.5 $mol \cdot L^{-1}$, the mesopore volume increased to 0.17 $cm^3 \cdot g^{-1}$ sharply. These facts indicate when HZSM-5 was treated with NaOH, mesopore structure can be introduced without damage to micropore structure on the condition of NaOH concentration lower than 0.3 $mol \cdot L^{-1}$, while behind this concentration, more mesopores will be made since the enhancement of desilication effect will lead to collapse of catalyst skeleton and reduction of micropores. Besides, combined to Table 1, it can be identified that alkali treatment of HZSM-5 with NaOH can introduce mesopores both on the external surface and inside the catalyst at the same time. For *x*TPA/Z5 series, there is no obvious change of micropore volume and surface area when the concentration of TPAOH solution is lower than 0.5 $mol \cdot L^{-1}$. However, with the increase of concentration, the mesopore volume keeps increasing. When the concentration reached to 0.5 $mol \cdot L^{-1}$, the micropore volume and surface area begin to decrease, while the mesopore volume is still increasing. This indicates that when the concentration does not exceed 0.4 $mol \cdot L^{-1}$, the mesopores can be introduced by desilication by organic alkali treatment while the structure of micropores can be protected. However, when the concentration of TPAOH exceeds 0.5 $mol \cdot L^{-1}$, too much skeleton silicon is removed by the alkali solution, which leads to the collapse of the catalyst skeleton and destroys of the micropores structure. To display mesopores generated after alkali treatment more intuitively, transmission electron microscopy (TEM) images of all the alkali-treated HZSM-5 are shown in Fig. S1 in Supplementary Material. It can be seen that after alkali treatment, the structure of the sample is not hollow as a whole, but many mesopores appear, and these mesopores appear as light-colored spots in TEM. Besides, NaOH-treated ZSM-5 samples have more and bigger mesopores. And with the increase of alkali concentrations, mesopores of either NaOH or TPAOH treated samples are getting more and more clear. However, mesopores of NaOH-treated samples are clearer than that of TPAOH-treated samples, which can be attributed to that TPAOH treated samples are thicker due to its weaker desilication ability. Comparing *x*TPA/Z5 to *x*Na/Z5 series, one can find the micropore volume and surface area of *x*TPA/Z5 is always higher when the alkali concentrations are identical. The reason is that compared to NaOH, the bigger molecule size of TPA^+ has gifted it stronger spatial steric resistance, which protected the catalysts from the attack of OH^-. Finally, the process of desilication was slowed down. Besides, the external surface area of *x*Na/Z5 catalysts are bigger, which implies the external surface of catalysts treated by NaOH is rougher, and the desilication of the external surface is obvious. On the other hand, the surface SiO_2/Al_2O_3 of *x*TPA/Z5 is obviously higher than

Table 2
Texture properties of HZSM-5 and HZSM-5 catalysts obtained by different post-treatments

Catalysts	Surface area/$m^2 \cdot g^{-1}$			Volume/$cm^3 \cdot g^{-1}$		
	BET	Micropore	External	Total	Micropore	Mesopore
HZSM-5	368	272	96	0.21	0.14	0.07
0.2Na/Z5	388	272	116	0.22	0.14	0.08
0.3Na/Z5	396	270	126	0.23	0.13	0.10
0.4Na/Z5	394	264	130	0.24	0.13	0.11
0.5Na/Z5	380	234	146	0.27	0.10	0.17
0.2TPA/Z5	378	273	105	0.22	0.14	0.08
0.3TPA/Z5	380	271	109	0.23	0.14	0.09
0.4TPA/Z5	386	270	116	0.24	0.14	0.10
0.5TPA/Z5	384	265	119	0.24	0.12	0.12
0.4TPA-24/Z5	397	271	126	0.30	0.14	0.16
Zn/Z5	334	261	73	0.20	0.13	0.07
Zn-0.4Na/Z5	357	260	97	0.21	0.13	0.08
Zn-0.4TPA/Z5	352	264	88	0.21	0.12	0.09
Zn-0.4TPA-24/Z5	358	266	92	0.27	0.13	0.14

bulk SiO_2/Al_2O_3, indicating TPA^+ can delay the removal of surface silicon species so that the hierarchical structure of micropores on the exterior surface and mesopores inside. For 0.4TPA-24/Z5 catalyst, the micropore surface area almost remains unchanged compared to 0.4TPA/Z5, while the total surface area increased by 10 $m^2 \cdot g^{-1}$ and mesopore volume increased by 0.06 $cm^3 \cdot g^{-1}$. This may be due to during the heating process of recrystallization, when the crystallization conditions of ZSM-5 have not been reached, the desiliconization reaction of the original ZSM-5 is still proceeding, so the mesopore volume and specific surface area of the zeolite will continue to increase, and the corresponding micropore volume reduction should occur. However, when the conditions of the system reach the crystallization conditions of ZSM-5, recrystallization takes over. At this time, the silicon and aluminum released due to TPAOH treatment form new ZSM-5 on the original zeolite surface, so the reduced micropore volume was supplemented again. In the end, the external surface area & mesopore volume increased for 0.4TPA-24/Z5 while no change in the micropore volume. This first identified the recrystallization by combining the mesopore volume change with SiO_2/Al_2O_3 change. Besides, it also implies the desilication caused by OH^- is happening inside the catalyst during recrystallization [29,35,36]. For Zn-loaded catalysts, the surface area and mesopores volume both decreased, which resulted from Zn species may cover some of the surfaces and blocking the pores [37–39]. However, for different catalysts, the degree of surface area and mesopores volume decline is not the same. The decrease of surface area and mesopores volume of Zn-0.4Na/Z5 is more than that of Zn-0.4TPA/Z5, which can be explained that more mesopores is existing on the outer surface of 0.4Na/Z5, and therefore, more Zn species are loaded inside the mesopores. While, the decrease of surface area and mesopores volume of Zn-0.4TPA-24/Z5 is more than that of Zn-0.4TPA/Z5, implying more Zn species is existing inside the pores of 0.4TPA-24/Z5. This can be further explained by the results of ICP-OES and XPS later.

3.2. Study of Zn loading and Zn state

To evaluate the effect of different pore structures on the loading of Zn, all the Zn-loaded catalysts were characterized by ICP-OES and XPS, and the result is shown in Table 3. The surface Zn content obtained by XPS was always higher than bulk Zn content obtained by ICP-OES, which indicates Zn is more easily enriched on the surface of the catalyst by the equal volume impregnation method. Among these catalysts, Zn-0.4Na/Z5 has the largest surface Zn content. This is because there are large amounts of mesopores on its surface, resulting in more Zn being loaded on the outer surface. Compared to Zn-0.4Na/Z5, the surface Zn content of Zn-0.4TPA/Z5 is lower. It can be explained by its fewer surface mesopores. While the surface Zn content of Zn-0.4TPA-24/Z5 is the lowest. This can be attributed to its low surface acid amount and good preservation of surface micropores structure. And it also indicates more Zn diffused into the interior channels of catalysts since there are more mesopores inside.

XPS spectra of Zn-modified catalysts with different textural properties are shown in Fig. 2. According to the literature, the curve was fitted to two characteristic peaks at 1021.9 eV and 1022.9 eV corresponding to ZnO and $ZnOH^+$, respectively [40–42]. Their specific contents calculated by integral are summarized in Table 4. As can be seen, the ratio of $ZnOH^+$/ZnO of different catalysts follows the sequence Zn-0.4Na/Z5>Zn-0.4TPA-24/Z5>Zn-0.4TPA/Z5>Zn/Z5. The highest $ZnOH^+$/ZnO ratio of Zn-0.4Na/Z5 is attributed to its rich mesoporous structure, in which the Zn tends to be evenly dispersed to form $ZnOH^+$, suppressing the formation of ZnO from enriched $ZnOH^+$. For 0.4TPA/Z5, though most of the mesopores are inside zeolite particles, some of the surface Si were also removed during desilication. Therefore, the mesopores on the surface of Zn-0.4TPA/Z5 are more than HZSM-5, which leads to higher $ZnOH^+$/ZnO. The $ZnOH^+$/ZnO ratio of Zn-0.4TPA-24/Z5 is 0.3 higher than that of Zn-0.4TPA/Z5 can be attributed to the decline of surface Brønsted acid density caused by recrystallization. The introduced Zn reacted more evenly with the reduced surface Brønsted acid to form more $ZnOH^+$ specie. Another worth mentioning fact is that though Zn-0.4TPA-24/Z5 did not possess the highest $ZnOH^+$ content, it revealed the highest amount of Lewis acid sites, which can be seen in Table 5. Since it is believed it is the formation of $ZnOH^+$ sites that converted Brønsted acid to Lewis acid, the mismatching of XPS results and acidity looks confusing. However, it can be interpreted as follows. XPS is a surface analysis method with a detection depth of only 3–10 nm, on Zn-0.4TPA-24/Z5, more Zn are distributed inside the zeolite. From the perspective of textural property, NaOH has strong desiliconization ability, the surface of the treated sample is relatively rough, and the mesopore distribution is relatively uniform. The TPA^+ ions in the TPAOH solution have a protective effect on the surface desiliconization of ZSM-5, and due to the existence of steric hindrance, the interior of ZSM-5 will be more attacked by OH^- ions. Therefore, the distribution of mesopores after TPAOH treatment is not uniform in space, and the parts close to the interior of the zeolite have more mesopores. Finally, from the perspective of acidity, indeed, $ZnOH^+$ sites act as Lewis acid sites, and the acidity from pyridine FTIR studies seems contradictory to the XPS results. But base on the above, we infer that $ZnOH^+$ is more likely to be generated in mesopores interior the zeolite. Therefore, the XPS analysis shows less $ZnOH^+$ on Zn-0.4TPA-24/Z5 but the pyridine FTIR study shows more Lewis acid sites.

Table 3
The zinc content of Zn-modified HZSM-5 catalyst with different pore structures

Catalysts	Zn/% (mass)	
	ICP	XPS
Zn/Z5	3.4	4.4
Zn-0.4Na/Z5	3.4	4.9
Zn-0.4TPA/Z5	3.4	4.6
Zn-0.4TPA-24/Z5	3.4	4.3

3.3. Acidity

NH_3-TPD was used to evaluate the acidity of the catalysts without metal loading, the profiles are in Fig. S2 to Fig. S4, and all the profiles can be separated into three peaks by fitting with the Gaussian function. In detail, temperature ranges of 180–220 °C, 220–320 °C and 320–550 °C were chosen to represent weak acid, medium acid, and strong acid in the fitting, respectively [43–46]. The data of acidity after fitting are shown in Table 6. For NaOH-treated catalysts, the total acid amount increased first and then decreased. It was proposed that the amount of exposed framework Al–OH was increased by desilication at low NaOH concentration, while it was decreased by the removal of structure Al at high NaOH concentration [47–49]. Besides, with the increase of NaOH concentration, the strong acid kept decreasing and the medium acid kept increasing, which indicates the framework Al was removed and formed non-framework species with medium acid strength. For catalysts treated with TPAOH, the amount of total acid sites increased with the concentration of TPAOH. This is also because the exposure of framework Al–OH can be promoted by desilication [50,51]. However, the rate of desilication at high TPAOH concentration was stable due to its steric hindrance, which resulted in the framework of zeolite can be better preserved to give more acid sites. For the recrystallized catalyst 0.4TPA-24/Z5, the total acid site

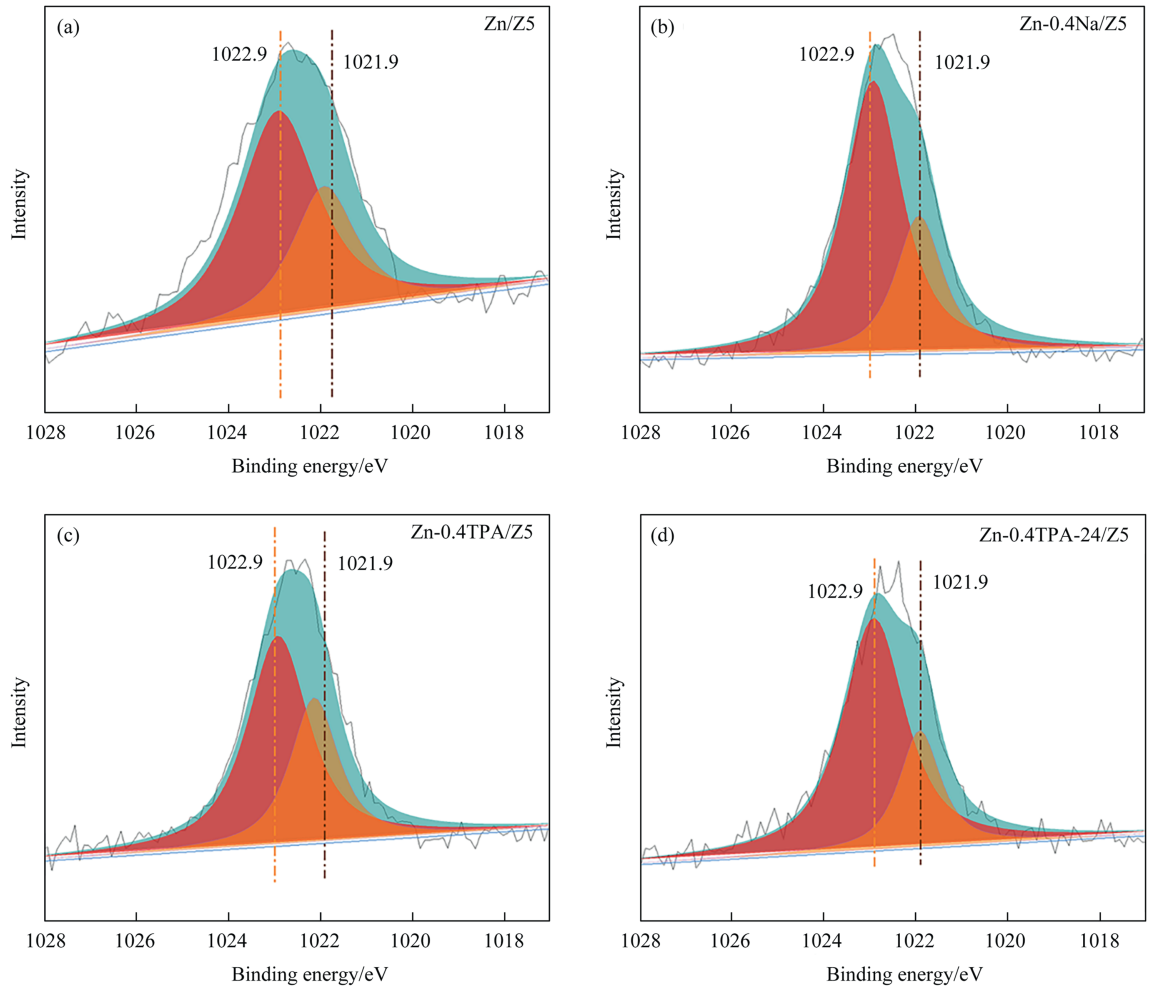

Fig. 2. Zn $2p_{3/2}$ XPS spectra of Zn-modified HZSM-5 catalyst with different pore structures.

Table 4
The distribution of the surface zinc state in Zn-modified HZSM-5 catalyst with different pore structures

Catalysts	$ZnOH^+$/% (mass) (1022.9 eV)	ZnO/% (mass) (1021.9 eV)	$ZnOH^+$/ZnO
Zn/Z5	3.0	1.4	2.1
Zn-0.4Na/Z5	3.6	1.3	2.8
Zn-0.4TPA/Z5	3.2	1.4	2.3
Zn-0.4TPA-24/Z5	3.1	1.2	2.6

is higher than that of 0.4Na/Z5 but lower than that of 0.4TPA/Z5. On one hand, the increased acid amount compared to 0.4Na/Z5 can be explained by the limited desilication by TPAOH. On the other hand, compared to 0.4TPA/Z5, the reduced acid amount is due to the recrystallization of desilicated Si species on the surface of zeolite would cover some of the Al—OH.

For Zn-modified catalysts with different pore structures, the spectrum of Py-IR is shown in Fig. 3, and the calculated Lewis acid amount (LAS) and Brønsted acid amount (BAS) is shown in Table 5. On non-modified ZSM-5 zeolite with SiO_2/Al_2O_3 ratio equals to 27, most of the acid sites are Brønsted acid. However, the introduction of Zn changes the acid type from Brønsted acid to Lewis acid, because the reaction of Zn with Brønsted acid creates $ZnOH^+$ species which exist in the way of Lewis acid. Therefore, the ratio of B/L dramatically decreased after the introduction of Zn. From Table 5, the amount of both LAS and BAS of Zn-0.4TPA/Z5 is higher than Zn-0.4Na/Z5. This is because the BAS content of 0.4TPA/Z5 was 99 $\mu mol \cdot g^{-1}$ more than that of 0.4Na/Z5, consequently, there is sufficient BAS to interact with Zn species to convert into LAS. The amount of LAS of Zn-0.4TPA-24/Z5 is 24 $\mu mol \cdot g^{-1}$ higher than that of Zn-0.4TPA/Z5. This is because more Zn species in Zn-0.4TPA-24/Z5 were loaded inside the catalyst and the $ZnOH^+$/ZnO on the outer surface was higher, which leads to more $ZnOH^+$ species exhibiting LAS were generated, and the LAS content increases. Although there are lots of BAS on 0.4TPA/Z5, its mesopores inside the catalyst were less than that of 0.4TPA-24/Z5. This leads to the uneven distribution of $ZnOH^+$ after the introduction of Zn, which would form ZnO after calcination and would reduce the amount of LAS.

3.4. Catalyst performances in 1-hexene aromatization

The 1-hexene aromatization is tested over the catalysts, the conversion, aromatic yield, and aromatic distribution for different catalysts are shown in Fig. 4, Fig. 5, Fig. 6 and Fig. 7. From the conversion results, it is clearly shown all the studied catalysts maintained high reactivity with 1-hexene conversion higher than 98.6% within 12 h TOS. And along the reaction period, a reduction of conversion appeared to all the catalysts, which can be attributed to the formation of coke on the acid sites hindered the reaction of 1-hexene.

Table 5
Acid types and acidic properties of Zn-modified HZSM-5 catalyst with different pore structures

Catalysts	Lewis acid amount/ μmol·g^{-1}			Brønsted acid amount/ μmol·g^{-1}		
	Total	Strong	Weak	Total	Strong	Weak
Zn/Z5	346	142	204	119	41	78
Zn-0.4Na/Z5	367	181	186	83	20	64
Zn-0.4TPA/Z5	376	239	137	94	41	52
Zn-0.4TPA-24/Z5	400	258	142	72	30	42

3.4.1. Performance of xNa/Z5 and xTPA/Z5 catalysts

For *x*Na/Z5 catalysts, as can be seen in Fig. 4(b), during the first 2 h TOS, aromatic yield first increased and then decreased with the increase of NaOH concentration. The maximum value of 33.9% (mass) was reached on 0.3Na/Z5. It can be attributed to more Al—OH being exposed by desilication, resulting in its highest total acid amount. Therefore, there are more active sites for 1-hexene to convert. On the other hand, comparing the reduction of aromatic yield (ΔA) during 2—12 h TOS, one can find the ΔA for alkali-treated catalysts is much less than that of HZSM-5. The ΔA follows the sequence 0.4Na/Z5<0.5Na/Z5<0.3Na/Z5<0.2Na/Z5<HZSM-5. It is proposed that the increase of mesopores after alkali treatment enhanced the diffusion of products inside the catalysts, and it further postponed the deactivation. Though 0.3Na/Z5 possessed the highest acid amount and the highest conversion in the first 2 h of TOS, the ratio of mesopore to total volume was only 43% (can be obtained from Table 2), less than it on 0.4Na/Z5 (46%). Therefore, the products can better diffuse in 0.4Na/Z5, with less ΔA of 3.2% (mass).

It is of great importance to evaluate the effect of catalysts' pore structure on the aromatic distribution, since benzene (B), toluene (T), and xylene (A8) are significant basic chemicals. Fig. 4(c) shows the aromatic distribution on *x*Na/Z5 catalysts when TOS = 12 h. One can find it is greatly affected by mesopore/total volume ratio. When mesopore/total volume ratio was less than 46%, the aromatics with carbon number no less than 9 (A9+) reduces with the increase of this ratio. From the aromatic distribution, it can be seen that the proportion of A9+ decreased with the increase of mesopore/total volume ratio until this ratio reaches 46%. It can be explained that the introduction of mesopores accelerates the diffusion of aromatic products and inhibits the further alkylation of small molecule aromatics, which can also be confirmed by that the proportion of B and T gradually increased with the increase of mesopore/total volume. In addition, the kinetic diameter of A8 is similar to that of the 10-membered ring pore of HZSM-5, and the micropores of HZSM-5 have a higher selectivity than A8. When mesopore/total volume increased to 46%, the proportion of A8 first increased due to the enhanced diffusion ability, and then decreased to 35.8% due to the decrease of A8 type selectivity due to the destruction of micropore structure of HZSM-5. While, when the mesopore/total volume increases from 46% to 63%, the distribution of aromatics with different carbon numbers basically did not change. But according to Fig. 4(a), it can be seen that the yield of aromatics decreased by 3.1% (mass). The further introduction of mesopores will not affect the distribution of aromatics in the product, but the yield of aromatics will decrease due to the collapse of the zeolite skeleton.

For *x*TPA/Z5 catalysts, as can be seen in Fig. 5(a), the conversion decreased with the increase of TOS. However, when TOS = 12 h, conversion on all the catalysts is still higher than 98.6%, and no obvious difference compared to *x*Na/Z5 catalysts. From the aspect of aromatic yield, from Fig. 5(b), one can tell though aromatic yields on all catalysts decreased with reaction time, 0.4TPA/Z5 always possessed the highest value. Comparing the ΔA from TOS = 2 h to TOS = 12 h on all the catalysts, it was found ΔA first increased and then decreased with the increase of TPAOH concentration, and 0.4TPA/Z5 possessed the minimum ΔA (10.0% (mass)). This indicates the stability of HZSM-5 can be enhanced by the introduction of mesopores. With the increase of TPAOH concentration, mesopore volume kept increasing, and the diffusion of products was facilitated in the catalysts. Nevertheless, when the concentration of TPAOH reached to 0.5 mol·L^{-1}, though the mesopore/total volume increased, the volume of micropores decreased. It suggests the microporous structure of the catalyst was damaged more or less, and the selectivity of catalyst micropores for aromatics decreased. Therefore, the ΔA increased.

Comparing Figs. 4(b) and Fig. 5(b), it was found whether it is 0.4 mol·L^{-1} NaOH or 0.4 mol·L^{-1} TPAOH, the post-treatment did enhance the stability and aromatization performance of the catalysts. During the whole reaction period, the ΔA on 0.4Na/Z5 (3.2% (mass)) was obviously lower than that on 0.4TPA/Z5 (10.0% (mass)). However, when TOS<6 h, the aromatics yield on 0.4TPA/Z5 was higher than 0.4Na/Z5. Especially when TOS = 2 h, the yield of aromatics on 0.4TPA/Z5 is 3.4% (mass) higher than that on 0.4Na/Z5. It is speculated that on one hand, the desilication rate of NaOH is faster than that of TPAOH, resulting in the collapse of the zeolite framework and the reduction of aromatics selectivity of the catalyst. Meanwhile, the reduction of acid amount on 0.4Na/Z5 caused by the removal of Al—OH during post-treatment reduced the active sites of aromatization may also result in the higher aromatics yield on 0.4TPA/Z5 when TOS<6 h. However, due to the diffusion constraints of TPA^+ in the channel of HZSM-5, it will absorb on the surface of the catalyst during the desilication and leave more micropores on the surface of 0.4TPA/Z5. Therefore, though the aromatics formed inside the catalyst can diffuse to the surface easily, the micropores on the surface will slow them down. In addition, there are abundant acidic sites on the outer surface of the catalyst. The aromatics will be transformed into by-products with bigger molecule sizes on the effect of both diffusion constraints and acidic sites, and finally, the by-products will block the channel of the catalyst and deactivate it.

Table 6
Acid properties of HZSM-5 and *x*Na/Z5 catalysts

Catalysts	Amount/μmol·g^{-1}				Proportion/%		
	Weak acid	Medium acid	Strong acid	Total acid	Weak acid	Medium acid	Strong acid
HZSM-5	287	42	239	568	50.5	7.4	42.1
0.2Na/Z5	292	55	235	582	50.2	9.4	40.4
0.3Na/Z5	306	68	216	590	51.8	11.5	36.6
0.4Na/Z5	284	72	184	540	52.7	13.2	34.1
0.5Na/Z5	262	86	154	511	51.2	16.8	30.1
0.2TPA/Z5	295	48	237	580	50.9	8.2	40.9
0.3TPA/Z5	297	50	239	586	50.7	8.5	40.8
0.4TPA/Z5	312	54	244	610	51.2	8.8	40.0
0.5TPA/Z5	325	75	228	628	51.7	12.0	36.3
0.4TPA-24/Z5	286	57	210	553	53.4	9.6	37.0

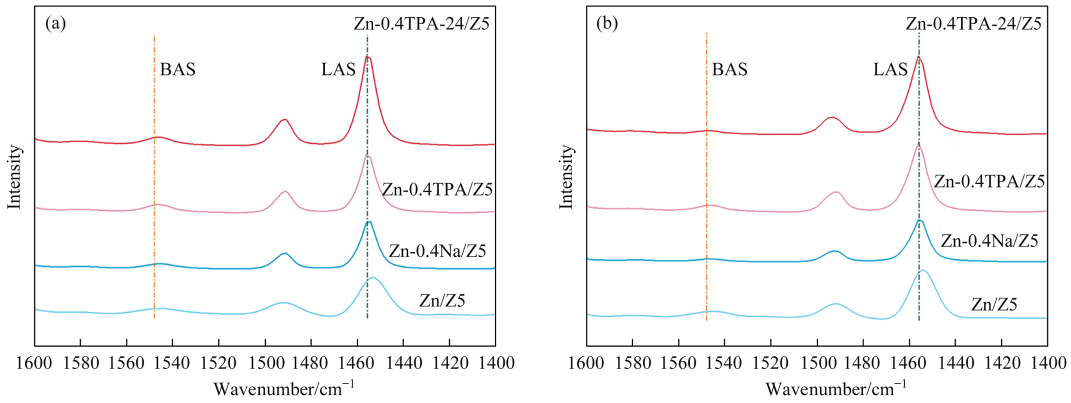

Fig. 3. Py-IR profiles of HZSM-5 and HZSM-5 catalysts obtained by different post-treatments adsorption at 200 °C (a) and 350 °C (b).

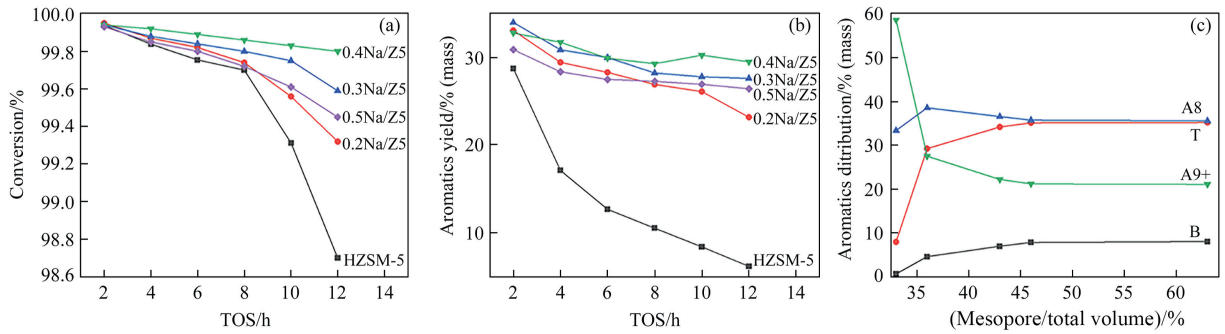

Fig. 4. (a) Conversion, (b) aromatization yield, and (c) aromatization distribution of 1-hexene aromatization over *x*Na/Z5 catalysts.

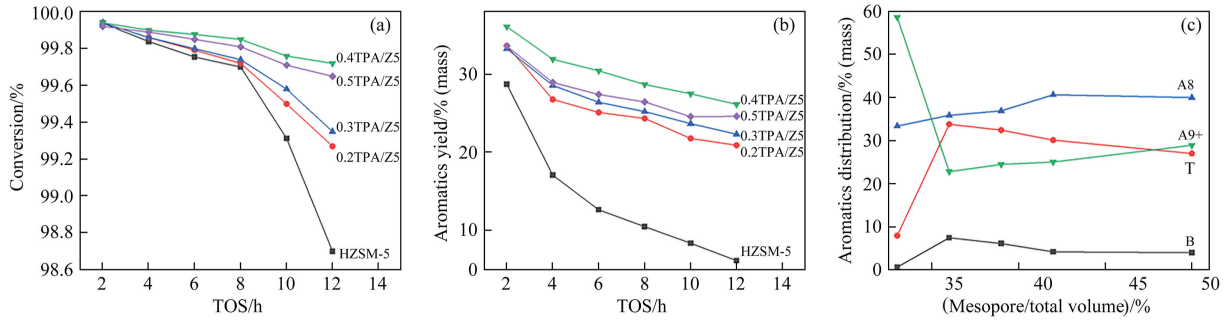

Fig. 5. (a) Conversion, (b) aromatization yield, and (c) aromatization distribution of 1-hexene aromatization over *x*TPA/Z5 catalysts.

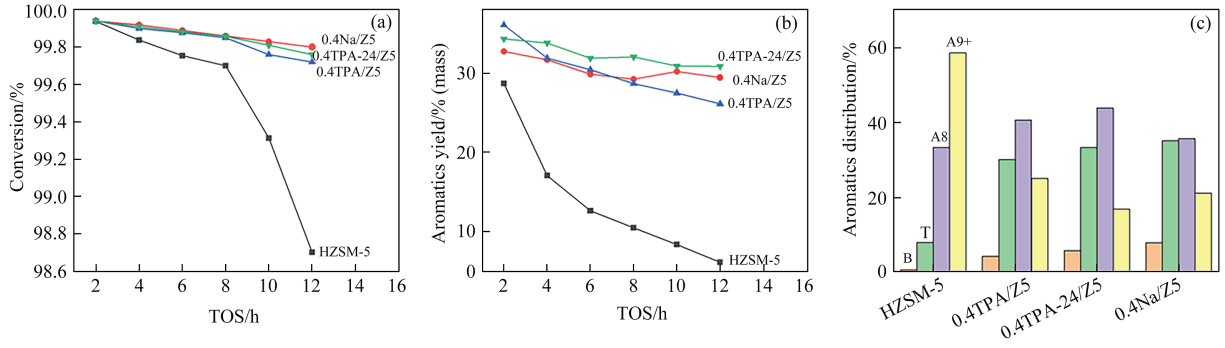

Fig. 6. (a) Conversion, (b) aromatization yield, and (c) aromatization distribution of 1-hexene aromatization over HZSM-5, 0.4TPA/Z5, 0.4TPA-24/Z5, and 0.4Na/Z5 catalysts.

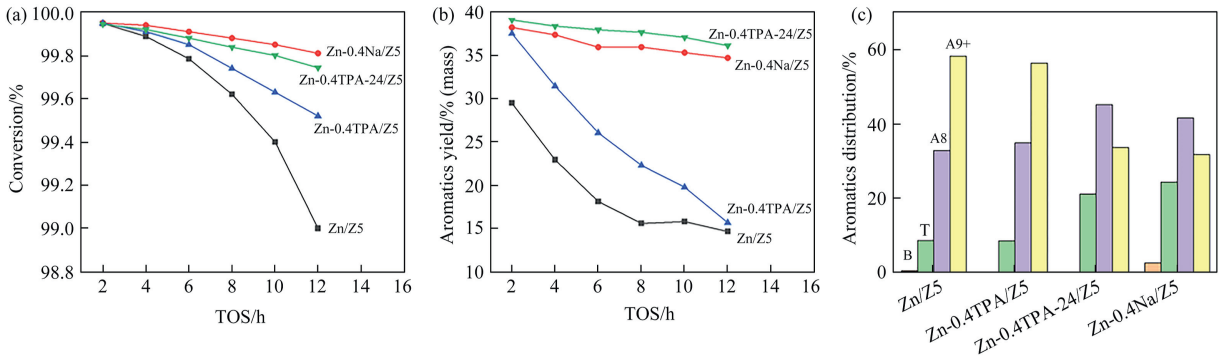

Fig. 7. (a) Conversion, (b) aromatization yield, and (c) aromatization distribution of 1-hexene aromatization over Zn-loaded catalysts.

To verify the conjecture, the aromatics distribution on *x*TPA/Z5 was further analyzed, as shown in Fig. 5(c), When mesopore/total volume is less than 36%, the introduction of mesopores enhanced the diffusion properties on products inside the catalysts, avoiding their further reaction to form bigger molecules. Therefore, the proportion of A9+ decreased and that of B, T, and A8 increased. When mesopore/total volume is higher than 36%, the proportion of A9+ and A8 increased and that of B and T decreased. This is because, on the one hand, as the concentration of TPAOH increases, more mesopores are formed inside the catalyst, which enhances the diffusion of small molecule aromatics to the outside of the catalyst. On the other hand, the surface of the catalyst is still protected by TPA^+, leaving a relatively intact microporous structure, which causes the diffusion of these small molecular aromatics to suddenly slow down on the surface and further react with the acidic sites. Because the molecular dynamics diameter of A8 is close to the pore diameter of HZSM-5, the pores on HZSM-5 have a higher selectivity to A8, so when the mesopore/total volume reaches 42%, the proportion of A8 still increases to the maximum value of 40.7%. When mesopore/total volume reaches 50%, the selectivity of A8 decreased, implying A8 will also react with the acid site around the micropore mouth to form A9+.

In conclusion, the introduction of mesopore will enhance the stability of the catalysts in 1-hexene aromatization. The difference between using NaOH and TPAOH is mainly reflected in A8 selectivity and the decrease in aromatics yield. The mesopores introduced by using NaOH are more uniform in the spatial distribution of the catalyst than those introduced by using TPAOH, so the stability is better. While more micropore structures are preserved by using TPAOH, resulting in its higher A8 selectivity. Therefore, how to prolong the lifetime of the catalyst while ensuring high A8 selectivity is very important. Because TPAOH is also an important template for the synthesis of HZSM-5 in addition to being an organic alkali, an attempt was made to replenish silicon and reduce acidity by recrystallizing the catalyst after TPAOH treatment.

3.4.2. Performance of 0.4TPA-24/Z5 catalyst

In Fig. 6, the 1-hexene aromatization performance of 0.4TPA-24/Z5 was compared to HZSM-5, 0.4Na/Z5, and 0.4TPA/Z5. From Fig. 6(b), at TOS = 2 h, the aromatics yield of 0.4TPA-24/Z5 is lower than that of 0.4TPA/Z5, but it's always higher than that of 0.4TPA/Z5 at TOS = 4–12 h. And its ΔA is only 3.4% (mass), which is much less than that of 0.4TPA/Z5 and very close to that of 0.4Na/Z5 (3.2% (mass)). This is because 0.4TPA/Z5 has the largest BAS amount, which is beneficial for the conversion of 1-hexene to aromatics in the early stages of the reaction. While the surface BAS amount of 0.4TPA-24/Z5 was reduced by the recrystallization, leading to the reduction of aromatics yield. With the increase of TOS, for 0.4TPA/Z5, the mesopores interior enhanced the diffusion of small molecule aromatics, but the large amount of BAS and micropores near the catalyst surface slowed them down and excess reactions occurred to deactivate the catalyst. While for 0.4TPA-24/Z5, not only are mesopores formed inside the catalyst, but also the SiO_2/Al_2O_3 ratio of the micropores on the surface decreases under the action of recrystallization, resulting in a decrease in the BAS content near the pore mouth, which inhibits the further reaction of aromatic molecules, thereby reducing the deactivation rate of the catalyst.

Fig. 6(c) shows the aromatics distribution at TOS = 12 h. It can be seen that HZSM- 5 possesses the highest percentage of A9+, which is resulted from there are more strong BAS on HZSM-5 and the proportion of micropores in the channels being relatively large, the diffusion rate of small molecular aromatics is slow, and under the action of strong BAS, alkylation reaction occurs to generate large molecular aromatics (A9+). After being treated by NaOH, the proportion of mesopores in the catalyst increased, and the diffusion of aromatics was enhanced, which inhibited the alkylation reaction, so the proportion of A9+ decreased, and the proportions of B, T, and A8 increased. However, after using TPAOH solution for post-treatment, the catalyst presents a structure with many internal mesoporous surfaces and few surface mesopores, and small molecular aromatics will accumulate near the pores to further react to form large molecular aromatics, so the proportion of A9+ increases to 25.1%. However, the micropore size on the surface of 0.4TPA/Z5 is similar to the kinetic diameter of A8, and the shape selectivity of A8 is better than that of 0.4Na/Z5, so the proportion of A8 increased from 35.8% to 40.7%. Compared with 0.4TPA/Z5, in 0.4TPA-24/Z5 after recrystallization treatment, the proportion of A9+ decreased from 25.1% to 16.7%, and the proportion of A8 further increased from 40.7% to 43.9%. The proportion of B and T also increased to 5.8% and 33.4%, respectively. This is because the silicon species dissolved by OH^- during the TPAOH solution treatment will exist in the form of silicate, and recrystallize on the surface of the catalyst, thereby reducing the BAS amount on the surface while protecting the micropore structure of the outer layer of the catalyst. Therefore, the alkylation reaction was suppressed since the small molecule aromatics accumulation near the pore mouth was inhibited due to the lack of acidic sites, so the proportion of A9+ further decreased while the proportions of B, T, and A8 increased.

3.4.3. Performance of Zn-loaded catalysts

In addition to pore structure, the acid properties of catalysts also play an important role in 1-hexene aromatization. In the research of 1-hexene aromatization, the acid properties of the catalyst are often adjusted by supporting metals (such as Zn) to increase the yield of aromatics. However, it is hard to find studies about the effect of the spatial distribution of mesopores on the loading of metal. Therefore, 3% (mass) Zn was loaded on HZSM-5, 0.4Na/Z5,

0.4TPA/Z5, and 0.4TPA-24/Z5. 1-Hexene aromatization of the synthesized catalysts was conducted.

Fig. 7 shows the performance of Zn-loaded catalysts. From Fig. 7(a), during the TOS from 0 to 12 h, the conversion of 1-hexene on all the catalysts is higher than 99%, indicating all the Zn-modified catalysts have high activity. Fig. 7(b) shows the yield of aromatization on TOS. Compared to Fig. 6(b), when TOS = 2 h, the yield on all the Zn-modified catalysts is higher than the counterpart without Zn loading. However, unlike the parent catalyst, the yield of aromatics on Zn-0.4TPA/Z5 decreases rapidly with the prolongation of TOS, which is similar to Zn/Z5. On one hand, this is because of the rather small mesopore volume of Zn-0.4TPA/Z5, which is only 0.08 $cm^3 \cdot g^{-1}$. At the same time, ZnO was formed inside the catalyst, which inhibited the diffusion of the products. On the other hand, the introduction of Zn has led to the increase of L/B, which is beneficial for the transformation of 1-hexene to aromatics. However, due to the ZnO inside the catalyst and on the pore mouth, it is harder for the aromatics to diffuse to the bulk phase, which led to the accumulation and further reaction of aromatics near the pore mouth on the surface of the catalyst and finally accelerated catalyst deactivation. While due to the higher mesopore volume and a higher proportion of $ZnOH^+$ on Zn-0.4TPA-24/Z5, the increased aromatics by the enhancement of L/B can diffuse inside the channel at a relatively high rate. In addition, the BAS amount near the pore mouth was reduced by recrystallization, which inhibited the further reaction of small molecule aromatics to coke. Therefore, the stability of this catalyst is higher. When TOS = 12 h, the aromatics yield on Zn-0.4TPA-24/Z5 is 20.0% (mass) higher than that on Zn/Z5. For Zn-0.4Na/Z5, there are plenty of mesopores inside and on the surface of the catalyst, so the accumulation at the pore mouth was avoided when the aromatics formed inside the catalyst diffused to the surface. Therefore, the aromatics yield loss is only 3.5% (mass) during TOS = 2–12 h. Nevertheless, the micropore structure could be destroyed by NaOH because of its too strong alkaline, which is not beneficial for aromatics selectivity, resulting in the aromatics yield on it is always lower than that on Zn-0.4TPA-24/Z5.

In addition to aromatics yield, we should also look into the aromatics distribution. Fig. 7(c) shows the proportion of aromatics with different carbon numbers of the products obtained by different catalysts when TOS = 12 h. It was found A9+ was the main product on Zn/Z5 and Zn-0.4TPA/Z5, which explains why it is easier to form coke to deactivate them. Due to the micropores with high A8 selectivity being preserved during TPAOH treatment, the surface BAS was reduced during recrystallization, and the Zn element exists in the form of $ZnOH^+$ inside the catalyst, the A8 proportion in the product obtained on Zn-0.4TPA-24/Z5 is 12.4% higher than it on Zn/Z5. At 12 h TOS, the proportion of A8 is still 43.9%, which is the maximum value among these 4 catalysts. For Zn-0.4Na/Z5, due to the plenty of mesopores formed under the function of NaOH solution, the diffusion of products was less limited and the alkylation reaction of small molecule aromatics near the pore mouth was suppressed; therefore, the proportion of A9+ reduced to 31.7% (mass). However, some of its micropore structure was destroyed by NaOH treatment with high concentration, so the proportion of A8 decreased by 3.6% (mass) compared to Zn-0.4TPA-24/Z5.

Apart from the above detailed aromatics distribution, the products distribution of all the hydrocarbons on Zn-0.4TPA-24/Z5 at TOS = 12 h was listed in Table S1 as group composition to illustrate what is also in the products besides aromatics.

4. Conclusions

HZSM-5 zeolite was post-treated with NaOH, TPAOH, and TPAOH then recrystallization to adjust its pore structure. It was found these three post-treatment protocols resulted in mesopores with different spatial distributions and affected the loading of Zn.

It was found mesopores were introduced evenly in spatial by the desilication function of NaOH solution. The evenly distributed mesopore was found beneficial to prolong the lifetime of catalyst, but unfavorable for enhancing the aromatics selectivity. This is due to the increase of mesopore volume, the diffusion of aromatics in the catalyst can be enhanced. On the other hand, the damage to micropores will result in a decrease in aromatic selectivity. And a balance was reached at the contration of 0.4 $mol \cdot L^{-1}$ NaOH.

For TPAOH-treated samples, the mesopores were preferentially introduced inside the catalyst other than on the surface. Besides, the desilication rate of TPAOH was much lower than NaOH, which resulted in a lower mesopore volume. However, the micropore structure can be better preserved by TPAOH treatment, which resulted in the maximum aromatic yield (26.1% (mass)) and maximum A8 selectivity (40.7%). To further improve the selectivity of xylene, 24-h recrystallization was conducted on 0.4TPA/Z5. It was found more mesopores were introduced and the micropores were well preserved. On the property of acidity, the recrystallized Si species on the surface have reduced the BAS amount near the pore mouth. Finally, the A8 selectivity was enhanced by 3.2% on 0.4TPA-24/Z5 compared to 0.4TPA/Z5. It was attributed to the synergy effect of mesopores spatial distribution and optimized acid properties.

It was found on the same Zn loading amount, catalyst with large amounts of mesopores on even spatial distribution favors the formation of $ZnOH^+$, which is beneficial for olefin aromatization. While the surface micropore favors the formation of ZnO, which will suppress the aromatization and stability. However, reducing the BAS amount near the pore mouth and increasing the mesopore volume inside the catalyst at the same time is beneficial for the entering of the Zn element into the interior of the catalyst. Thus, more $ZnOH^+$ was formed to enhance the stability and selectivity of A8. And the formation of A9+ aromatics was suppressed by the unique pore structure.

The findings presented here significantly broaden the view of how mesopores in Zn/HZSM-5 catalyst affect the selectivity of xylene in 1-hexene aromatization.

Declaration of Interest

The authors declare that they have no known competing financial interests or personal relationships that could have appeared to influence the work reported in this paper.

Acknowledgements

This work was supported by National Natural Science Foundation of China (22021004).

Supplementary Material

Supplementary data to this article can be found online at https://doi.org/10.1016/j.cjche.2023.11.008.

References

[1] K. Yan, Y.Y. Yang, J.J. Chai, Y.R. Lu, Catalytic reactions of gamma-valerolactone: A platform to fuels and value-added chemicals, *Appl. Catal., B* 179 (2015) 292–304.
[2] J. Ren, F. Xin, Y.S. Xu, A review on direct synthesis of dimethoxymethane, *Chin. J. Chem. Eng.* 50 (2022) 43–55.
[3] D. Jampaiah, D.Y. Murzin, A.F. Lee, D. Schaller, S.K. Bhargava, B. Tabulo, K. Wilson, Catalytic selective ring opening of polyaromatics for cleaner transportation fuels, *Energy Environ. Sci.* 15 (5) (2022) 1760–1804.
[4] M. Raad, A. Astafan, S. Hamieh, J. Toufaily, T. Hamieh, J.D. Comparot, C. Canaff, T.J. Daou, J. Patarin, L. Pinard, Catalytic properties of Ga-containing MFI-type

zeolite in cyclohexane dehydrogenation and propane aromatization, *J. Catal.* 365 (2018) 376–390.
[5] H.M. Lapa, L.M.D.R.S. Martins, *p*-Xylene oxidation to terephthalic acid: New trends, *Molecules* 28 (4) (2023) 1922.
[6] Y.X. Wang, T. Biddle, C.L. Jiang, T. Luong, R.J. Chen, S. Brown, X.Y. Jie, J.L. Hu, Microwave-driven upcycling of single-use plastics using zeolite catalyst, *Chem. Eng. J.* 465 (2023) 142918.
[7] W.W. Kaeding, C. Chu, L.B. Young, B. Weinstein, S.A. Butter, Selective alkylation of toluene with methanol to produce *para*-xylene, *J. Catal.* 67 (1) (1981) 159–174.
[8] L. Young, Shape selective reactions with zeolite catalysts III. Selectivity in xylene isomerization, toluene-methanol alkylation, and toluene disproportionation over ZSM-5 zeolite catalysts, *J. Catal.* 76 (2) (1982) 418–432.
[9] J.A. Biscardi, G.D. Meitzner, E. Iglesia, Structure and density of active Zn species in Zn/H-ZSM5 propane aromatization catalysts, *J. Catal.* 179 (1) (1998) 192–202.
[10] J. Zhu, W.T. Wu, Y. Chang, X.H. Sun, H.Y. Wang, Application of nano-HZSM-5 catalyst on aromatization of FCC gasoline, *Petrol. Sci. Technol.* 28 (1) (2010) 7–12.
[11] H.X. Wang, G. Hu, H. Lei, Y.D. Xu, X.H. Bao, A facile and effective method for the distribution of Mo/HZSM-5 catalyst active centers, *Catal. Lett.* 89 (1) (2003) 75–79.
[12] Y.M. Jia, J.W. Wang, K. Zhang, C.M. Ding, Highly shape-selective Zn-P/HZSM-5 zeolite catalyst for methanol conversion to light aromatics, *Appl. Organomet. Chem.* 34 (11) (2020) e5932.
[13] X.H. Yang, F. Wang, R.P. Wei, S. Li, Y.F. Wu, P.X. Shen, H.Z. Wang, L.J. Gao, G.M. Xiao, Synergy effect between hierarchical structured and Sn-modified H[Sn, Al]ZSM-5 zeolites on the catalysts for glycerol aromatization, *Microporous Mesoporous Mater.* 257 (2018) 154–161.
[14] Y.B. Xu, Y. Song, X.H. Liu, Z.G. Zhang, Effect of bed height on the performance of a fixed Mo/HZSM-5 bed in direct aromatization of methane, *Chem. Eng. Technol.* 39 (11) (2016) 2059–2065.
[15] J.C. Groen, W.D. Zhu, S. Brouwer, S.J. Huynink, F. Kapteijn, J.A. Moulijn, J. Pérez-Ramírez, Direct demonstration of enhanced diffusion in mesoporous ZSM-5 zeolite obtained *via* controlled desilication, *J. Am. Chem. Soc.* 129 (2) (2007) 355–360.
[16] Y.N. Li, S.L. Liu, Z.K. Zhang, S.J. Xie, X.X. Zhu, L.Y. Xu, Aromatization and isomerization of 1-hexene over alkali-treated HZSM-5 zeolites: Improved reaction stability, *Appl. Catal., A* 338 (1–2) (2008) 100–113.
[17] H.Y. Long, F.Y. Jin, G. Xiong, X.S. Wang, Effect of lanthanum and phosphorus on the aromatization activity of Zn/ZSM-5 in FCC gasoline upgrading, *Microporous Mesoporous Mater.* 198 (2014) 29–34.
[18] L. Lin, X.T. Zhang, N. He, J.X. Liu, Q. Xin, H.C. Guo, Operando dual beam FTIR study of hydroxyl groups and Zn species over defective HZSM-5 zeolite supported zinc catalysts, *Catalysts* 9 (1) (2019) 100.
[19] J.E. Gao, C.L. Wei, M. Dong, G.F. Wang, Z.K. Li, Z.F. Qin, J.G. Wang, W.B. Fan, Evolution of Zn species on Zn/HZSM-5 catalyst under H_2 pretreated and its effect on ethylene aromatization, *ChemCatChem* 11 (16) (2019) 3892–3902.
[20] J.X. Liu, N. He, W. Zhou, L. Lin, G.D. Liu, C.Y. Liu, J.L. Wang, Q. Xin, G. Xiong, H.C. Guo, Isobutane aromatization over a complete Lewis acid Zn/HZSM-5 zeolite catalyst: Performance and mechanism, *Catal. Sci. Technol.* 8 (16) (2018) 4018–4029.
[21] D. Gao, Y.B. Zhi, L.Y. Cao, L. Zhao, J.S. Gao, C.M. Xu, M.Z. Ma, P.F. Hao, Influence of zinc state on the catalyst properties of Zn/HZSM-5 zeolite in 1-hexene aromatization and cyclohexane dehydrogenation, *Chin. J. Chem. Eng.* 43 (2022) 124–134.
[22] Q. Li, W.W. Cong, C.Y. Xu, S.G. Zhang, F. Wang, D.Z. Han, G.J. Wang, L.C. Bing, New insight into the inductive effect of various seeds on the template-free synthesis of ZSM-5 zeolite, *CrystEngComm* 23 (48) (2021) 8641–8649.
[23] Y. Liu, S.Y. Han, D.D. Guan, S. Chen, Y.H. Wu, Y. Yang, N.Z. Jiang, Rapid green synthesis of ZSM-5 zeolite from leached illite clay, *Microporous Mesoporous Mater.* 280 (2019) 324–330.
[24] A. Javdani, J. Ahmadpour, F. Yaripour, Nano-sized ZSM-5 zeolite synthesized *via* seeding technique for methanol conversions: A review, *Microporous Mesoporous Mater.* 284 (2019) 443–458.
[25] T. Biemelt, C. Selzer, F. Schmidt, G. Mondin, A. Seifert, K. Pinkert, S. Spange, T. Gemming, S. Kaskel, Hierarchical porous zeolite ZSM-58 derived by desilication and desilication re-assembly, *Microporous Mesoporous Mater.* 187 (2014) 114–124.
[26] K. Tarach, K. Góra-Marek, J. Tekla, K. Brylewska, J. Datka, K. Mlekodaj, W. Makowski, M.C. Igualada López, J. Martínez Triguero, F. Rey, Catalytic cracking performance of alkaline-treated zeolite Beta in the terms of acid sites properties and their accessibility, *J. Catal.* 312 (2014) 46–57.
[27] K. Sadowska, A. Wach, Z. Olejniczak, P. Kuśtrowski, J. Datka, Hierarchic zeolites: zeolite ZSM-5 desilicated with NaOH and NaOH/tetrabutylamine hydroxide, *Microporous Mesoporous Mater.* 167 (2013) 82–88.
[28] M.J. Verhoef, P.J. Kooyman, J.C. van der Waal, M.S. Rigutto, J.A. Peters, H. van Bekkum, Partial transformation of MCM-41 material into zeolites: Formation of nanosized MFI type crystallites, *Chem. Mater.* 13 (2) (2001) 683–687.
[29] Z. Ma, T.J. Fu, Y.J. Wang, J.A. Shao, Q.A. Ma, C.M. Zhang, L.P. Cui, Z. Li, Silicalite-1 derivational desilication-recrystallization to prepare hollow nano-ZSM-5 and highly mesoporous micro-ZSM-5 catalyst for methanol to hydrocarbons, *Ind. Eng. Chem. Res.* 58 (6) (2019) 2146–2158.
[30] S.S. Arzumanov, A.A. Gabrienko, A.V. Toktarev, Z.N. Lashchinskaya, D. Freude, J. Haase, A.G. Stepanov, Propane transformation on Zn-modified zeolite. Effect of the nature of Zn species on alkane aromatization and hydrogenolysis, *J. Phys. Chem. C* 123 (50) (2019) 30473–30485.
[31] A. Bonnin, J.D. Comparot, Y. Pouilloux, V. Coupard, D. Uzio, L. Pinard, Mechanisms of aromatization of dilute ethylene on HZSM-5 and on Zn/HZSM-5 catalysts, *Appl. Catal., A* 611 (2021) 117974.
[32] A. Shahid, A. Inayat, Y. Avadhut, M. Hartmann, W. Schwieger, A comparative study of the desilication of channel- and cage-like zeolites, *Microporous Mesoporous Mater.* 341 (2022) 111903.
[33] D.Z. Zhang, C.Z. Jin, M.M. Zou, S.J. Huang, Mesopore engineering for well-defined mesoporosity in Al-rich aluminosilicate zeolites, *Chemistry* 25 (11) (2019) 2675–2683.
[34] S.T. Yang, C.X. Yu, L.L. Yu, S. Miao, M.M. Zou, C.Z. Jin, D.Z. Zhang, L.Y. Xu, S.J. Huang, Bridging dealumination and desilication for the synthesis of hierarchical MFI zeolites, *Angew. Chem. Int. Ed.* 56 (41) (2017) 12553–12556.
[35] T.J. Fu, Z. Ma, Y.J. Wang, J. Shao, Q. Ma, C.M. Zhang, L.P. Cui, Z. Li, Si/Al ratio induced structure evolution during desilication-recrystallization of silicalite-1 to synthesize nano-ZSM-5 catalyst for MTH reaction, *Fuel Process. Technol.* 194 (2019) 106122.
[36] J.J. Li, M. Liu, X.W. Guo, S. Zeng, S.T. Xu, Y.X. Wei, Z.M. Liu, C.S. Song, Influence of Al coordinates on hierarchical structure and T atoms redistribution during base leaching of ZSM-5, *Ind. Eng. Chem. Res.* 57 (45) (2018) 15375–15384.
[37] J. Álvarez-Rodríguez, I. Rodríguez-Ramos, A. Guerrero-Ruiz, A. Arcoya, Surface changes in Ru/KL supported catalysts induced by the preparation method and their effect on the selective hydrogenation of citral, *Appl. Catal., A* 366 (1) (2009) 114–121.
[38] A. Godelitsas, T. Armbruster, HEU-type zeolites modified by transition elements and lead, *Microporous Mesoporous Mater.* 61 (1–3) (2003) 3–24.
[39] J. Álvarez-Rodríguez, I. Rodríguez-Ramos, A. Guerrero-Ruiz, E. Gallegos-Suarez, A. Arcoya, Influence of the nature of support on Ru-supported catalysts for selective hydrogenation of citral, *Chem. Eng. J.* 204–206 (2012) 169–178.
[40] P. He, J.S. Jarvis, S.J. Meng, Q.Y. Li, G.M. Bernard, L.J. Liu, X.H. Mao, Z. Jiang, H.B. Zeng, V.K. Michaelis, H. Song, Co-aromatization of methane with propane over Zn/HZSM-5: The methane reaction pathway and the effect of Zn distribution, *Appl. Catal., B* 250 (2019) 99–111.
[41] X.J. Niu, J. Gao, K. Wang, Q. Miao, M. Dong, G.F. Wang, W.B. Fan, Z.F. Qin, J.G. Wang, Influence of crystal size on the catalytic performance of H-ZSM-5 and Zn/H-ZSM-5 in the conversion of methanol to aromatics, *Fuel Process, Technol.* 157 (2017) 99–107.
[42] A. Bonnin, Y. Pouilloux, V. Coupard, D. Uzio, L. Pinard, Deactivation mechanism and regeneration study of Zn/HZSM-5 catalyst in ethylene transformation, *Appl. Catal., A* 611 (2021) 117976.
[43] X.N. Han, H.Z. Li, H.K. Huang, L. Zhao, L.Y. Cao, Y.X. Wang, J.S. Gao, C.M. Xu, Effect of olefin and aromatics on thiophene adsorption desulfurization over modified NiY zeolites by metal Pd, *RSC Adv.* 6 (78) (2016) 75006–75013.
[44] C.L. Wen, J.D. Xu, X.M. Wang, Y. Fan, *n*-Nonane hydroisomerization over hierarchical SAPO-11-based catalysts with sodium dodecylbenzene sulfonate as a dispersant, *Petrol. Sci.* 18 (2) (2021) 654–666.
[45] H.Z. Li, L.X. Dong, L.A. Zhao, L.Y. Cao, J.S. Gao, C.M. Xu, Enhanced adsorption desulfurization performance over mesoporous ZSM-5 by alkali treatment, *Ind. Eng. Chem. Res.* 56 (14) (2017) 3813–3821.
[46] T. Pan, Z.J. Wu, K.Y. Zhou, *In situ* incorporation of Zn into hierarchical ZSM-5 zeolites for olefin hydroisomerization, *Ind. Eng. Chem. Res.* 59 (27) (2020) 12371–12380.
[47] W. Qin, Y.W. Zhou, J.D. Rimer, Deleterious effects of non-framework Al species on the catalytic performance of ZSM-5 crystals synthesized at low temperature, *React. Chem. Eng.* 4 (11) (2019) 1957–1968.
[48] T. Biligetu, Y. Wang, T. Nishitoba, R. Otomo, S. Park, H. Mochizuki, J.N. Kondo, T. Tatsumi, T. Yokoi, Al distribution and catalytic performance of ZSM-5 zeolites synthesized with various alcohols, *J. Catal.* 353 (2017) 1–10.
[49] P. Sazama, B. Wichterlova, J. Dedecek, Z. Tvaruzkova, Z. Musilova, L. Palumbo, S. Sklenak, O. Gonsiorova, FTIR and ^{27}Al MAS NMR analysis of the effect of framework Al- and Si-defects in micro- and micro-mesoporous H-ZSM-5 on conversion of methanol to hydrocarbons, *Microporous Mesoporous Mater.* 143 (1) (2011) 87–96.
[50] B. Hu, W.X. Chen, X.J. Wang, G.L. Mao, M.J. Luo, Etching behavior of TEAOH in the post-synthesis of hierarchical SAPO-34, *Res. Chem. Intermed.* 49 (2) (2023) 619–634.
[51] L. Treps, C. Demaret, D. Wisser, B. Harbuzaru, A. Méthivier, E. Guillon, D.V. Benedis, A. Gomez, T. de Bruin, M. Rivallan, L. Catita, A. Lesage, C. Chizallet, Spectroscopic expression of the external surface sites of H-ZSM-5, *J. Phys. Chem. C* 125 (3) (2021) 2163–2181.